

IMPLEMENTATION AND VALIDATION OF THE DIRECT METHOD FOR EFFECTIVE SIMULATION OF DYNAMIC DAM-FOUNDATION INTERACTION

D. Froio¹ & F. Carnevale²

¹ ISMES S.p.a., Bergamo, Italy, diego.froio@ismes.it

² ISMES S.p.a., Bergamo, Italy

Abstract: *For the seismic analysis of dams, the spatial variation of the ground motion around the underlying canyon, generated by Dynamic Soil-Structure Interaction (DSSI), may introduce differential displacements, possibly detrimental for the stability of high dams. The Direct Method (DM) is the most general procedure to numerically simulate the local spatial variation of the ground motion, when performing both linear and nonlinear seismic DSSI analyses. This method relies on the availability of special Free-Field Boundaries (FFBs), which shall input the seismic wave train and simultaneously absorb outgoing waves at the artificial boundary of the adopted FEM model. However, FFBs are seldom implemented by default in most commercial FEM codes. An original implementation of the DM in Comsol Multiphysics is here presented and validated against available analytical solutions. The present work demonstrates that rigorous DSSI analyses can be correctly performed in the above-mentioned mechanical context, even by using standard FEM programs, once the FFBs are correctly implemented and handled.*

1. Introduction

A detailed study of the seismic risk is mandatory for large dam plants located in seismically active regions. One of the crucial aspects for a realistic seismic analysis of a dam is the simulation of the complex wave mechanism induced by Dynamic Soil-Structure Interaction (DSSI). When an incident seismic wave front impinges the dam-foundation interface, wave diffraction occurs due to the inability of such interface to conform to the wave field. Scattered (reflected and diffracted) waves are spread into the surrounding soil without coming back. Seismic waves setting the dam into vibration, once reflected, are also radiated into the soil, thus introducing additional waves within the foundation. Since the motion of the dam depends on that of the foundation and vice versa, the DSSI phenomenon is fully coupled.

The numerical simulation, e.g. by the Finite Element Method (FEM), of DSSI phenomena poses several complications due to the need of materializing an artificial border, so called interaction horizon (Wolf, 1988), where truncating the spatial extension of the model. The computational strategy for handling the unbounded domain not included into the FEM model (far-field) is the main and unique difference among the two main families of methods for simulating DSSI: the Substructure Method (SM) and the Direct Method (DM).

The application of the DM and of its variants has been gradually spreading in dam engineering practice since the last decade. The main practical advantages of the DM as compared to the SM are the following. In the DM the effect of the omitted far-field is reproduced by imposing local Absorbing Boundary Conditions (ABCs) along the artificial boundary of the numerical model. Such transmitting boundaries are devised to approximate the radiation condition, i.e. to limit the wave reflection at the artificial boundary. The simplest of such ABCs is the

well-known viscous boundary of Lysmer and Kuhlemeyer (1969), which is available in the most of commercial FEM computer program. Instead, the SM needs boundary integral techniques to calculate the dynamic stiffness matrix of the unbounded far-field (Wolf, 1985; Chopra, 2020), such as the Boundary Element Method (BEM), which are seldom available in commercial software for structural analysis. Moreover, the DM also allows to simulate the nonlinear behavior of the dam and of the neighboring foundation (near-field) in the time domain, as opposed to the SM, being usually formulated in frequency domain and, thus, requiring a linear behavior of the dam, the reservoir and the foundation.

When the dynamic loading is directly applied within the computational domain, the only scope of an ABC is to transmit outgoing waves out from the numerical model. Froio et al. (2019) showed that the latter case occurs when implementing the DM under the condition of a spatially uniform Ground Motion (GM) in the absence of the structure, as traditionally assumed in the seismic assessment of dams. Nevertheless, the matter becomes more intricate when the spatial variation of the GM caused by the seismic wave passage must be accounted for, as the truncation boundary should allow the incoming seismic wave to enter the model without any modification as well as to ensure that scattered waves are absorbed. Standard ABCs are not able to accomplish this task. Thus, when the excitation originates from outside of the model in the form of incoming seismic waves, the formulation of the ABCs needs to be modified.

Since the shear wave velocities of the earth's surface lie in the range from about 0.1 km/s to about 3 km/s and the strong earthquake shaking of interest falls in the frequency range from about 0.1 Hz to about 20 Hz, the corresponding wavelengths are from tens of meters to tens of kilometres (Sánchez-Sesma, 1987). Then, for a dam footprint having dimensions near to the wavelengths associated with the most important periods of the GM, appreciable variations of GM amplitudes and phases occur along the dam-foundation interface even in the absence of the dam. The spatial variation (incoherence) of the GM caused by local site topography and geology may have significant effects on the seismic GM and, thus, are of particular significance for either the assessment of the seismic risk of existing dams or the planning and seismic design of new important hydroelectric facilities.

The seismic amplification conveyed by ridges and canyons, so-called site effect, has long been recognized as significant. The observations based on available strong motion records near the dam footprint during earthquakes have shown the GM is far from being uniform, especially at its higher frequency components, as reported by Hall (1988), Alves and Hall (2006), Chopra (2012) and more recently by Koufoudi et al. (2018). The outcomes of numerical models implementing either the SM (Szczesniak et al., 1999; Maeso et al., 2002; Chopra and Wang, 2010; Wang and Chopra, 2010) or the DM (Løkke and Chopra, 2017-2019; Jin et al., 2019; Sotoudeh et al., 2019; Varmazyari and Sabbagh-Yazdi, 2021) have confirmed that the spatial nonuniformity of the GM produced by vertically propagating incoming seismic waves has an appreciable influence on the structural response of dams.

A forthright application of the DM in the realm of finite elements under the assumption of a vertical propagation of the seismic waves was possible by the introduction of the Free-Field Boundary (FFB) devised by Zienkiewicz et al. (1989). The basic idea of the FFB is to augment the numerical model with free-field columns and planes to separately calculate the vertically propagating incident seismic wave field, so that its absorption by any ABC acting on different elevations of the artificial boundary can be prevented, as explained in the following Section 2. However, at present FFBs are not available by default in most of the commercial FEM codes commonly used for the seismic analysis of dams. To fill this gap, this paper illustrates an original and convenient computational strategy to model the FFB into COMSOL Multiphysics®. To the authors' best knowledge, no similar approach has been accomplished before by this FEM software. The robustness and accuracy of the present implementation are confirmed through a consistent validation process based on two benchmark problems whose analytical solution is well-known. Hence, the present work demonstrates that the spatial variability of the GM caused by vertically propagating seismic waves can be rigorously simulated using standard FEM programs once the FFBs are correctly implemented and handled.

The present paper is organized as follows. The formulation of the DM for linear DSSI analysis is the subject of Section 2, whereas its implementation in COMSOL Multiphysics® is presented in Section 3. The validation analyses are discussed in Section 4. Conclusive considerations of this work are summarized in final Section 5.

2. General formulation of the Direct Method

In the present section, the formulation of DSSI is discussed with reference to an arbitrary three-dimensional linear soil-structure system. The extension of the explained formulation to nonlinear problems entails minor modifications (see e.g. Aydinoglu, 1993).

Let consider the general scheme portrayed in Figure 1. The generalized structure, denoted by capital letter \hat{S} , includes the structure (S) and the near-field (N), that is the neighboring foundation enclosing all the material inhomogeneities of the soil, possibly exhibiting a nonlinear behavior. The far-field (F), i.e. the soil-structure system deprived by the generalized structure, is conceived as a semi-unbounded domain possibly having a countable set of layers. The geometry of the far-field, i.e. the shape of the free-surface and of the interfaces between the layers, if any, is assumed to extend towards infinity along the normal direction to the so-called *interaction horizon* Γ_h (Wolf, 1988), the latter being the ideal interface between the generalized structure and the far-field. The mechanical properties of the far-field may vary with depth, but they are assumed to be uniform within each individual layer. The layers are made of isotropic linear viscoelastic materials, except for the bottom homogeneous linear elastic half-space (seismic bedrock), which is traditionally assumed to be undamped.

The location of the interaction horizon is in charge to the analyst, depending on the characteristics of the DSSI problem at hand and on the adopted methodology to solve it. Since part of the scattered wave field is quite always reflected at Γ_h due to the faulty absorption abilities of any local ABC, the generalized structure must always include an adequate volume of the neighbouring soil. Moreover, a reliable simulation of the nonlinear response of the generalized structure can be only attained by placing the interaction horizon sufficiently far away from the structure, so that the linear elastic behaviour of the far-field can be justified.

Although any numerical method apt to spatially discretize the governing equations of motion of the dam-foundation system may be considered, the FEM is usually adopted by virtue of its capabilities to deal with embedment effects as well as any other geometrical or mechanical inhomogeneity quite easily. Thus, the generalized structure is here discretized as an assembly of finite elements.

Let \mathbf{u}^t be the total displacements vector obtained from a FEM discretization of the system, where the adjective “total” means that displacements are evaluated with respect to a fixed coordinate system. The displacements of the generalized structure are included into $\mathbf{u}_u^t = \{\mathbf{u}_s^t, \mathbf{u}_i^t, \mathbf{u}_g^t\}^T$, the nodal displacements of the interaction horizon are identified by \mathbf{u}_h^t , whereas the far-field displacements are pointed out by \mathbf{u}_f^t . Clearly, all previously introduced displacement vectors depends on time variable t .

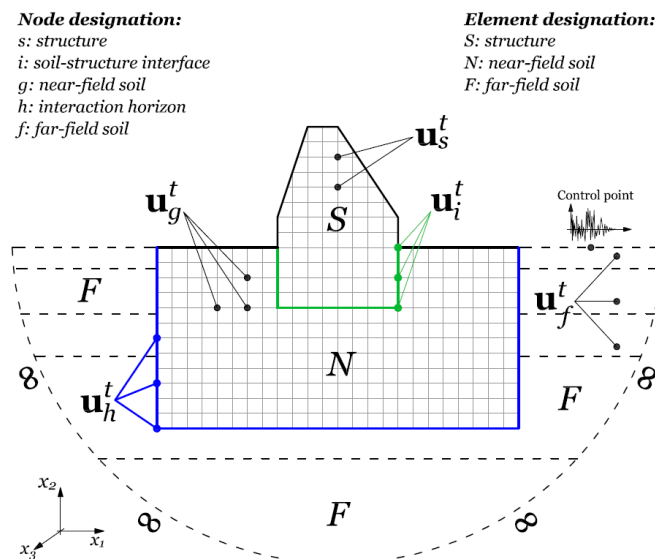


Figure 1. General scheme and notation of the DSSI problem.

By performing a dynamic condensation of the contribution of far-field degrees of freedom (f), the linear equations of motion of a viscously damped soil-structure system in the frequency domain read (Wolf, 1985):

$$\begin{bmatrix} \bar{\mathbf{K}}_{uu} & \bar{\mathbf{K}}_{uh} \\ \bar{\mathbf{K}}_{hu} & \bar{\mathbf{K}}_{hh}^s + \bar{\mathbf{S}}_{hh}^F \end{bmatrix} \begin{Bmatrix} \bar{\mathbf{u}}_u^t \\ \bar{\mathbf{u}}_h^t \end{Bmatrix} = \begin{Bmatrix} \mathbf{0} \\ \bar{\mathbf{S}}_{hh}^F \bar{\mathbf{u}}_h^g \end{Bmatrix}; \quad (1)$$

where $\bar{\mathbf{u}}^t = \{\bar{\mathbf{u}}_u^t, \bar{\mathbf{u}}_h^t\}^T$ is the Fourier transform of $\mathbf{u}^t = \{\mathbf{u}_u^t, \mathbf{u}_h^t\}^T$, $\bar{\mathbf{K}}_{kl} = \mathbf{K}_{kl} + i\omega\mathbf{C}_{kl} - \omega^2\mathbf{M}_{kl}$ is the dynamic stiffness (impedance) submatrix relating the degrees of freedom (dofs) k and l , \mathbf{K}_{kl} , \mathbf{C}_{kl} and \mathbf{M}_{kl} are the stiffness, damping and mass submatrices, respectively, ω is the angular frequency and

$$\bar{\mathbf{S}}_{hh}^F = \bar{\mathbf{K}}_{hh}^F + \bar{\mathbf{K}}_{hf} \bar{\mathbf{K}}_{ff}^{-1} \bar{\mathbf{K}}_{fh}; \quad (2)$$

is the condensed dynamic stiffness matrix of the far-field, expressing the radiation condition enforced by such unbounded linear viscoelastic domain at the dofs ensuing from the FEM discretization of Γ_h . Vector $\bar{\mathbf{u}}_h^g$ in Eq. (1) is the response of the far-field evaluated at the interaction horizon that would occur in the absence of the generalized structure (Wolf, 1985).

The seismic loading of the soil-structure system on the rhs of Eq. (1) can be evaluated once $\bar{\mathbf{u}}_h^g$ is available. Following a well-established practice in seismic engineering, far-field response $\bar{\mathbf{u}}_h^g$ is usually replaced by so-called Free-Field Motion $\bar{\mathbf{u}}_h^f$ (FFM), i.e. the response of a viscoelastic layered half-space obtained by projecting towards infinity the geometry of the interaction horizon. The main advantage of using $\bar{\mathbf{u}}_h^f$ in place of $\bar{\mathbf{u}}_h^g$ is that the first response can be calculated from simpler analytical/numerical approaches than those required to calculate $\bar{\mathbf{u}}_h^g$, especially under the usual assumption of vertical propagation of the seismic waves. The impedance of the FF half-space is here denoted by $\bar{\mathbf{S}}_{hh}^H$.

Substituting the relationships existing between $\bar{\mathbf{u}}_h^g$ and $\bar{\mathbf{u}}_h^f$ (Wolf, 1985):

$$\bar{\mathbf{S}}_{hh}^H \bar{\mathbf{u}}_h^f = \bar{\mathbf{S}}_{hh}^F \bar{\mathbf{u}}_h^g; \quad (3)$$

into Eq. (1), the following system is obtained

$$\begin{bmatrix} \bar{\mathbf{K}}_{uu} & \bar{\mathbf{K}}_{uh} \\ \bar{\mathbf{K}}_{hu} & \bar{\mathbf{K}}_{hh}^s + \bar{\mathbf{S}}_{hh}^F \end{bmatrix} \begin{Bmatrix} \bar{\mathbf{u}}_u^t \\ \bar{\mathbf{u}}_h^t \end{Bmatrix} = \begin{Bmatrix} \mathbf{0} \\ \bar{\mathbf{S}}_{hh}^H \bar{\mathbf{u}}_h^f \end{Bmatrix}; \quad (4)$$

expressing the equations of motion of DSSI with the FFM determining the load vector. According to the previous equation, the load vector is expressed as the product between the dynamic stiffness matrix of the FF, condensed at the nodes belonging to the interaction horizon where the generalized structure is assembled, and the FFM of the same nodes.

Finally, let $\bar{\mathbf{F}}_h^f$ be the integral of free-field stresses $\bar{\boldsymbol{\sigma}}^f$ over the finite element discretization of Γ_h :

$$\bar{\mathbf{F}}_h^f = \int_{\Gamma_h} \mathbf{N}_h^T \bar{\boldsymbol{\sigma}}^f(\mathbf{u}_h^f) \cdot \mathbf{n} \, dS; \quad (5)$$

where \mathbf{N}_h is the $3 \times 3N_h$ matrix of global shape functions restricted to Γ_h (N_h is the total number of nodes belonging to the mesh of Γ_h) and \mathbf{n} is its normal vector. Then, by equilibrium one has (Wolf, 1988)

$$\bar{\mathbf{F}}_h^f + \bar{\mathbf{S}}_{hh}^F \mathbf{u}_h^f = \bar{\mathbf{S}}_{hh}^H \mathbf{u}_h^f; \quad (6)$$

which, once substituted into Eq. (4), determines the following final system of equations:

$$\begin{bmatrix} \bar{\mathbf{K}}_{uu} & \bar{\mathbf{K}}_{uh} \\ \bar{\mathbf{K}}_{hu} & \bar{\mathbf{K}}_{hh}^s + \bar{\mathbf{S}}_{hh}^F \end{bmatrix} \begin{Bmatrix} \bar{\mathbf{u}}_u^t \\ \bar{\mathbf{u}}_h^t \end{Bmatrix} = \begin{Bmatrix} \mathbf{0} \\ \bar{\mathbf{S}}_{hh}^F \bar{\mathbf{u}}_h^f + \bar{\mathbf{F}}_h^f \end{Bmatrix}. \quad (7)$$

A schematic representation of Eq. (7) and its physical interpretation is given in Figure 2. Notice that the radiation condition of the far-field, transposed in numerical terms by matrix $\bar{\mathbf{S}}_{hh}^F$, applies to motion $\bar{\mathbf{u}}_h^t - \bar{\mathbf{u}}_h^f$ arising from the waves scattered by the generalized structure. As compared to Eq. (4), Eq. (7) has the advantage of not requiring the assembly of matrix $\bar{\mathbf{S}}_{hh}^H$, but on the other hand it requires the computation of both FF displacements and boundary tractions.

The time domain version of Eq. (7) is obtained owing to the Convolution Theorem:

$$\begin{bmatrix} \mathbf{M}_{uu} & \mathbf{M}_{uh} \\ \mathbf{M}_{hu} & \mathbf{M}_{hh}^s \end{bmatrix} \begin{Bmatrix} \ddot{\mathbf{u}}_u^t \\ \ddot{\mathbf{u}}_h^t \end{Bmatrix} + \begin{bmatrix} \mathbf{C}_{uu} & \mathbf{C}_{uh} \\ \mathbf{C}_{hu} & \mathbf{C}_{hh}^s \end{bmatrix} \begin{Bmatrix} \dot{\mathbf{u}}_u^t \\ \dot{\mathbf{u}}_h^t \end{Bmatrix} + \begin{bmatrix} \mathbf{K}_{uu} & \mathbf{K}_{uh} \\ \mathbf{K}_{hu} & \mathbf{K}_{hh}^s \end{bmatrix} \begin{Bmatrix} \mathbf{u}_u^t \\ \mathbf{u}_h^t \end{Bmatrix} + \left\{ \int_0^t \mathbf{S}_{hh}^F(t-\tau)(\mathbf{u}_h^t - \mathbf{u}_h^f) d\tau \right\} = \begin{Bmatrix} \mathbf{0} \\ \mathbf{F}_h^f \end{Bmatrix}; \quad (8)$$

where $\mathbf{S}_{hh}^F(t)$ is the Inverse Fourier Transform of impedance matrix $\bar{\mathbf{S}}_{hh}^F(\omega)$ and the overdot is the adopted notation for a time derivative. Eq. (8) forms the reference formulation of the DM in the time domain.

In the DM the radiation condition is approximated by imposing local ABCs along the interaction horizon. The local property of an ABCs means that the enforced boundary condition involves the responses of at most few points in the neighbourhood of the boundary point under consideration within a relatively small time-window. This is opposed to the exact radiation condition of Eq. (8), where the reaction-displacement relation along Γ_h is given by a convolution integral (nonlocal in time) of a dense matrix-vector product (nonlocal in space). Numerous ABCs have been proposed in the literature, such as the viscous boundary, the paraxial boundary, the DtN map, the Perfectly Matched Layer, etc.. For the DSSI analysis procedure described in the following section the viscous boundary is selected owing to its availability in almost any commercial FEM code, acceptable accuracy and ease of implementation.

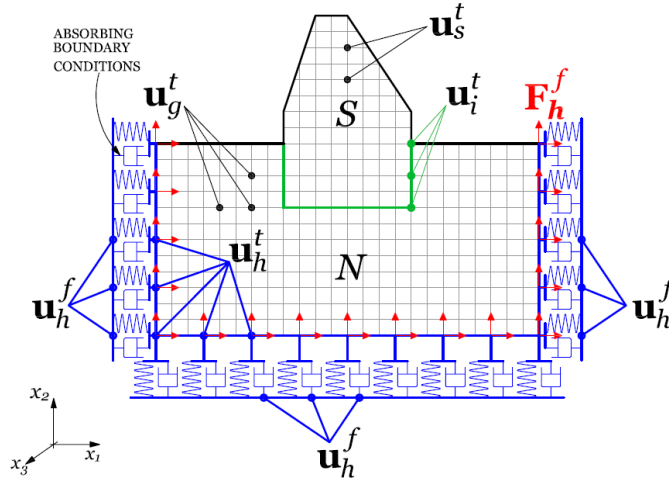


Figure 2. Schematic model, notation and physical interpretation of the DM.

3. Implementation of the DM in Comsol Multiphysics®

Let consider the scheme of a three-dimensional dam-foundation system shown in Figure 3. The unbounded foundation domain is truncated by a box-shaped artificial boundary (interaction horizon) having its faces oriented as the fixed cartesian axes x, y, z . Only the upper free surface of the model tracing the real topography of the valley may depart from flat geometry.

Let Γ_{hk} be the subset of Γ_h having normal parallel to the k -axis. By applying the viscous boundary of Lysmer and Kuhlemeyer (1969), the exact radiation condition in Eq. (8) is approximated as follows:

$$\int_0^t \mathbf{S}_{hh}^F(t-\tau)(\mathbf{u}_h^t - \mathbf{u}_h^f) d\tau \approx (\mathbf{C}_{hh}^{F,x} + \mathbf{C}_{hh}^{F,y} + \mathbf{C}_{hh}^{F,z})(\dot{\mathbf{u}}_h^t - \dot{\mathbf{u}}_h^f) = \mathbf{C}_{hh}^F(\dot{\mathbf{u}}_h^t - \dot{\mathbf{u}}_h^f); \quad (9)$$

where

$$\begin{aligned} \mathbf{C}_{hh}^{F,x} &= \int_{\Gamma_{hx}} \mathbf{N}_h^T \rho \text{diag}(\{c_{(P)}, c_{(S)}, c_{(S)}\}) \mathbf{N}_h dS, & \mathbf{C}_{hh}^{F,y} &= \int_{\Gamma_{hy}} \mathbf{N}_h^T \rho \text{diag}(\{c_{(S)}, c_{(P)}, c_{(S)}\}) \mathbf{N}_h dS, \\ \mathbf{C}_{hh}^{F,z} &= \int_{\Gamma_{hz}} \mathbf{N}_h^T \rho \text{diag}(\{c_{(S)}, c_{(S)}, c_{(P)}\}) \mathbf{N}_h dS; \end{aligned} \quad (10)$$

are the damping matrices ensuing from the distributed viscous dashpots placed on the vertical faces and on the horizontal bottom face of the interaction horizon, ρ is the far-field mass density, $c_{(S)}$ and $c_{(P)}$ are its shear wave and pressure wave velocities, respectively, and $\text{diag}(\mathbf{d})$ denotes a diagonal matrix having vector \mathbf{d} on its main diagonal.

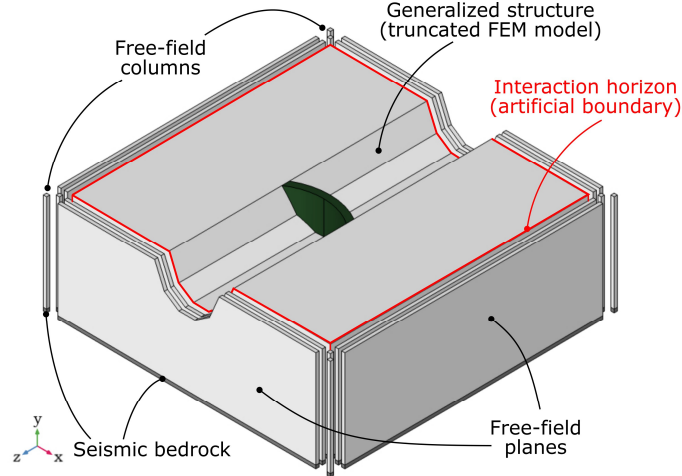


Figure 3. General arrangement of the computational model implementing the DM in Comsol Multiphysics®.

The viscous boundary given by Eq. (9) should be interpreted as an approximation of the exact radiation condition, which is usually accurate for practical engineering purposes provided that the extension of the near-field is sufficiently large. Since the wave absorption capabilities of viscous boundaries downgrade for oblique angles of incidence, it is advisable to leave a relatively large margin between the interaction horizon and the portion of the generalized structure whose response is of interest.

Substitution of Eq. (9) into Eq. (7) and Eq. (8) yields the final equations of motion of the DM including the viscous boundary as the adopted ABC:

$$\begin{bmatrix} \bar{\mathbf{K}}_{uu} & \bar{\mathbf{K}}_{uh} \\ \bar{\mathbf{K}}_{hu} & \bar{\mathbf{K}}_{hh}^s + i\omega \mathbf{C}_{hh}^F \end{bmatrix} \begin{Bmatrix} \bar{\mathbf{u}}_u^t \\ \bar{\mathbf{u}}_h^t \end{Bmatrix} = \begin{Bmatrix} \mathbf{0} \\ \bar{\mathbf{P}}_h^f \end{Bmatrix}, \quad (11a)$$

$$\begin{bmatrix} \mathbf{M}_{uu} & \mathbf{M}_{uh} \\ \mathbf{M}_{hu} & \mathbf{M}_{hh}^s \end{bmatrix} \begin{Bmatrix} \ddot{\mathbf{u}}_u^t \\ \ddot{\mathbf{u}}_h^t \end{Bmatrix} + \begin{bmatrix} \mathbf{C}_{uu} & \mathbf{C}_{uh} \\ \mathbf{C}_{hu} & \mathbf{C}_{hh}^s + \mathbf{C}_{hh}^F \end{bmatrix} \begin{Bmatrix} \dot{\mathbf{u}}_u^t \\ \dot{\mathbf{u}}_h^t \end{Bmatrix} + \begin{bmatrix} \mathbf{K}_{uu} & \mathbf{K}_{uh} \\ \mathbf{K}_{hu} & \mathbf{K}_{hh}^s \end{bmatrix} \begin{Bmatrix} \mathbf{u}_u^t \\ \mathbf{u}_h^t \end{Bmatrix} = \begin{Bmatrix} \mathbf{0} \\ \mathbf{P}_h^f \end{Bmatrix}; \quad (11b)$$

in the frequency domain and in the time domain, respectively, where

$$\mathbf{P}_h^f = \mathbf{C}_{hh}^F \dot{\mathbf{u}}_h^f + \mathbf{F}_h^f; \quad (12)$$

are the so-called effective earthquake forces (Løkke and Chopra, 2017 and 2018).

Hence, the boundary tractions acting on the interaction horizon are made of two contributions. The first contribution are boundary reactions $-\mathbf{C}_{hh}^F (\dot{\mathbf{u}}_h^t - \dot{\mathbf{u}}_h^f)$ of the viscous dashpots to the scattered motion only, thus leaving the FFM unaffected. The second contribution originates from traction resultants \mathbf{F}_h^f of the FFM. The latter term may also include the reaction forces ensuing from any pre-existing static loads acting on the generalized structure. A FFB is any boundary condition capable of providing both actions on Γ_h .

The calculation of FF velocities $\dot{\mathbf{u}}_h^f$ and traction resultants \mathbf{F}_h^f must rely on the definition of a suitable numerical model of the FF problem. Under the usual and pragmatic hypothesis of a seismic wave field consisting of plane SH-, SV-, and P-waves vertically propagating upwards from the underlying semi-unbounded foundation (Chopra, 2020), the FF system can be modelled by at most eight planar layers and eight FF columns added to the computational model of the generalized structure, as shown in Figure 3. Both FF layers and columns are also discretized by finite elements with the same mesh density of the generalized structure.

Twin FF layers (or planes) are introduced for each vertical face of the interaction horizon, sharing the same in-plane geometry and stratigraphy of Γ_h . Each layer simulates the FF response of the half-space obtained by projecting towards infinity the geometry of the corresponding vertical face of Γ_h along its normal direction. Two layers are needed for each vertical face of Γ_h because two different sets of boundary conditions must be enforced to reproduce the out-of-plane (SH-wave field) and the in-plane (SV- and P-wave fields) half-space motion. In particular, the following BCs must be prescribed at any FF layer with outer normal \mathbf{n}_k ($k = x, z$):

$$\mathbf{u}^f - (\mathbf{u}^f \cdot \mathbf{n}_k) \mathbf{n}_k = 0, \quad \text{for out-of-plane motion}; \quad (13a)$$

$$\mathbf{u}^f \cdot \mathbf{n}_k = 0, \quad \text{for in-plane motion;} \quad (13b)$$

where $\mathbf{u}^f = \{u_x^f, u_y^f, u_z^f\}^T$ is the three-dimensional FF displacement vector.

Since any FF layer is a truncated model of a semi-infinite half-space, its vertical boundaries must be also endowed with FFBs. Towards this scope, twin FF columns are located at each corners of the FEM model to reproduce the FF response of a flat half-space sharing the same stratigraphy of the adjacent FF layers, which is assumed to indefinitely extend in both horizontal directions. Then, two FF columns must be added at each model corner to impose the following two distinct sets of BCs at all nodes of a FF column:

$$u_y^f = 0, \quad \text{for S-wave vertical propagation;} \quad (14a)$$

$$u_x^f = u_z^f = 0, \quad \text{for P-wave vertical propagation;} \quad (14b)$$

when simulating vertical wave propagation by finite elements. The first of Eqs. (14) prevents any bending effect of the FF column, so that its dynamic response is compelled to display a pure shear deformation; the second of Eqs. (14) inhibits any unwanted Poisson's effect associated with the column axial vibration.

The parts of the FF model are highlighted in the Figure 4. The seismic response of the FF model is processed in parallel with that of the generalized structure as the dynamic analysis advances either in the time or in the frequency domains. The FF response must be independent from that of the generalized structure. In fact, the FF system is, by definition, a regular half-space located at an unbounded distance from the generalized structure and, thus, it cannot be reached by the waves scattered by the generalized structure. On the contrary, the FF response ($\hat{\mathbf{u}}_h^f$ and \mathbf{F}_h^f) calculated by each FF column are mapped to the lateral boundaries of the adjacent FF planes by using the *General Extrusion* ("genext") nonlocal coupling function available in Comsol Multiphysics®. Likewise, $\hat{\mathbf{u}}_h^f$ and \mathbf{F}_h^f calculated within the domain of each FF layer are mapped to the corresponding lateral face of the interaction horizon by means of the same coupling function. Hence, the information travels from the FF columns to the FF layers, and from the FF layers to the generalized structure, but never in the opposite way.

Finally, the effective earthquake forces applied at the bottom boundary of the model must be calculated. Currently, the standard approach in dam engineering is to define the earthquake as a suite of three orthogonal acceleration components $a_x^{oc}(t), a_y^{oc}(t), a_z^{oc}(t)$ describing the motion of an outcrop point, i.e. a control point located at the rock surface (Figure 1) where strong-motion earthquakes are normally recorded (Wolf, 1985). The spectra of such acceleration components should, in some sense not examined here, be consistent with a target spectrum representing the seismic hazard of the site, which is usually derived according to either a deterministic or a probabilistic seismic hazard analysis (Kramer, 1996).

Since seismic hazard analysis typically does not consider local site effects, such as topography and stratigraphy, an outcrop signal is intended as the surface motion of a reference flat half-space. Displacement field u^h of a flat half-space excited by solely plane SH-, SV- and P-waves propagating in the vertical direction (y), is given by the solution of the well-known one-dimensional wave equation (Wolf, 1985; Kramer, 1996):

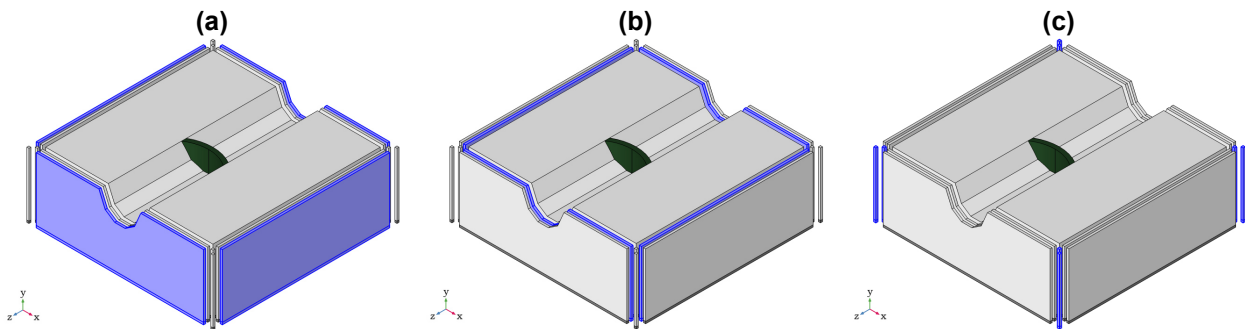


Figure 4. Components of the model required for computing FF displacements and traction resultants: vertical layers for computing the out-of-plane (a) and the in-plane (b) components of the FFM at the lateral artificial boundary of the generalized structure; corner columns for computing the FFM at the lateral artificial boundaries of the vertical layers (c).

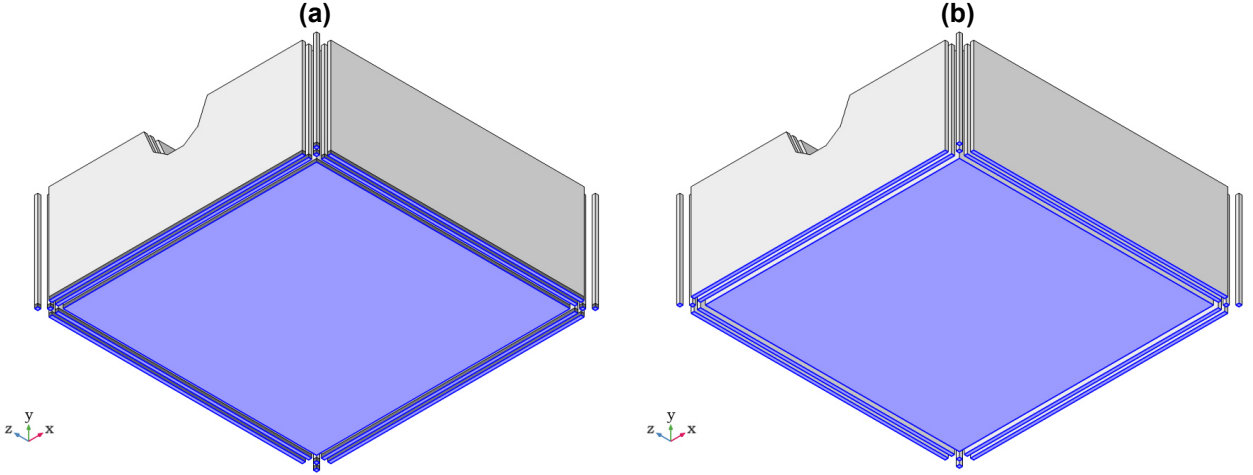


Figure 5. Bottom horizontal face of the interaction horizon where the ABC is enforced (a) and reference plane where effective earthquake forces are applied (b).

$$u_k^h(y, t) = u_k^{hl}(ct - y) + u_k^{ho}(ct + y); \quad (15)$$

where u_k^{hl} and u_k^{ho} denotes the incoming (incident) and outgoing (reflected) wave fields, and $c = c_{(p)}$ in the case of pressure waves ($k = y$) or $c = c_{(s)}$ in the case of shear waves ($k = x, z$).

Within the assumed reference frame ($y > 0$ if upward), the radiation condition at any depth y provides the following expression of the boundary traction for a unit normal \mathbf{n} pointing in the negative y -direction:

$$f_k^{hl} = \sigma_{kl}^{hl}(\mathbf{u}^{hl})n_l = c\rho\dot{u}_k^{hl}, \quad f_k^{ho} = \sigma_{kl}^{ho}(\mathbf{u}^{ho})n_l = -c\rho\dot{u}_k^{ho}. \quad (16)$$

whose resultants over the FEM discretization of the horizontal boundary $y = y_0$ is

$$\mathbf{F}_h^{h,y} = \int_{\Gamma_{hy}} \mathbf{N}_h^T \mathbf{f}^{h0} dS = \int_{\Gamma_{hy}} \mathbf{N}_h^T \rho \text{diag}(\{c_{(s)}, c_{(p)}, c_{(s)}\}) (2\dot{\mathbf{u}}^{h10} - \dot{\mathbf{u}}^{h0}) dS = \mathbf{C}_{hh}^{F,y} (2\dot{\mathbf{u}}^{h10} - \dot{\mathbf{u}}^{h0}); \quad (17)$$

where $\dot{\mathbf{u}}^{h0} = \dot{\mathbf{u}}^h(y_0, t)$. Thus, by imposing that FF stress resultants at the bottom boundary $\mathbf{F}_h^{f,y}$ is equal to $\mathbf{F}_h^{h,y}$, i.e. $\mathbf{u}^{f0} = \mathbf{u}^{h0}$, the outcrop motion would be recovered at the free surface of the generalized structure when the latter coincides with the reference flat half-space. Recalling Eq. (12), this in turn implies that the effective earthquake forces to be applied at the bottom boundary are

$$\mathbf{P}_h^{f,y} = 2\mathbf{C}_{hh}^{F,y} \dot{\mathbf{u}}^{f10}. \quad (18)$$

The FF incoming wave velocities $\dot{\mathbf{u}}^{f10}$ at a given depth must be consistently defined to obtain the surface control motion $\mathbf{a}^{oc}(t)$ at the surface of a one-dimensional column representing the reference half-space. This task can be accomplished by performing a one-dimensional deconvolution analysis of the outcrop motion (Løkke and Chopra, 2017). When specifying the earthquake excitation in this way, the spatial variation of the GM is automatically considered in the numerical analysis, albeit predominantly in the vertical direction.

Effective earthquake forces $\mathbf{P}_h^{f,y}$ do not need to act at the bottom boundary, where ABCs are enforced. Instead, they can be theoretically applied along any horizontal plane in between the bottom artificial boundary of the model and the highest depth below which the near-field can be guaranteed being regular, i.e. constituted by horizontal layers made of linear viscoelastic materials. In fact, it may happen sometimes that the application of external forces badly interacts with the behaviour of the adopted ABC. If this is the case, the effective earthquake forces may be applied to a horizontal surface just above the bottom face of the artificial boundary, as illustrated in Figure 5. Although this paper illustrates a Comsol Multiphysics® realisation, the procedure herein presented is equally valid and adaptable to other commercial FEM codes if a coupling functionality analogous to the *General Extrusion* are made available.

4. Validation of the numerical results

This section illustrates the results of several numerical experiments carried out to verify the correct functioning of the present implementation of the DM. The evaluation of the consistency and accuracy of the proposed methodology is based on the comparison between the computed displacement at the foundation surface for two benchmark problems, whose exact analytical solutions are available in the literature. The analytical solutions of both benchmark problems have been implemented in the MatLab environment.

The first benchmark problem, discussed in Section 4.1, consist in calculating the surface amplification of a planar wave vertically propagating into a homogeneous viscously damped elastic layer resting on a viscoelastic half-space. The second benchmark problem, presented in the subsequent Section 4.2 pertains the scattering of a train of SH harmonic waves propagating in the vertical direction carried out by a semi-cylindrical canyon located at the free surface of a half-space.

4.1. Vertical propagation of a harmonic plane S-wave in a viscoelastic layer on an elastic half-space

Let consider a homogeneous soil/rock deposit of depth H made of an isotropic, linear viscoelastic material behaving according to the following Kelvin-Voigt (KV) model:

$$\tau = G_s \gamma + \eta_s \dot{\gamma}, \quad \tau_{(KV)s} = \frac{\eta_s}{G_s}; \quad (19)$$

where $\tau = \sigma_{12}$ is the shear stress, $\gamma = 2\varepsilon_{12} = u_{1,2}$ is the shear strain, G_s and η_s are the material shear modulus and viscosity of the layer, respectively, and $\tau_{(KV)s}$ is the characteristic time scale governing the behaviour of the KV unit. Thus, the shear stress is given by the sum of an elastic part, proportional to the shear strain, and a viscous part, proportional to the shear strain rate. The shear wave velocity of the soil layer is denoted by $c_{(S)s}$, whereas its mass density is ρ_s . The soil layer rests on an elastic bedrock having a shear wave velocity of $c_{(S)b}$ and a mass density of ρ_b .

The soil layer is subjected to vertically propagating harmonic plane S-waves coming from the bedrock, with unitary amplitude at the surface and circular frequency ω . The S-waves are polarized along the x -axis.

The complex-valued transfer function of the system, i.e. the ratio between free surface motion of the soil layer and the bedrock outcropping motion, is given by the following formula:

$$F(\hat{\omega}_s^*, \alpha^*) = \frac{1}{\cos(\hat{\omega}_s^*) + i\alpha^* \sin(\hat{\omega}_s^*)}; \quad (20)$$

where

$$\hat{\omega}_s^* = \frac{\omega H}{c_{(S)s} \sqrt{1 + i\omega \tau_{(KV)s}}} = \frac{\hat{\omega}_s}{\sqrt{1 + i\hat{\omega}_s \hat{\tau}_{(KV)s}}}; \quad (21a)$$

$$\alpha^* = \frac{\rho_s c_{(S)s}}{\rho_b c_{(S)b}} \sqrt{1 + i\omega \tau_{(KV)s}} = \alpha \sqrt{1 + i\hat{\omega}_s \hat{\tau}_{(KV)s}}; \quad (21b)$$

are the complex nondimensional frequency and the complex impedance ratio, respectively. Transfer function F depends on real impedance ratio $\alpha = \rho_s c_{Ss} / \rho_b c_{Sb}$ of the undamped system ($\tau_{(KV)s} = 0$), on the nondimensional frequency of the layer $\hat{\omega}_s = \omega H / c_{(S)s}$ and on the nondimensional characteristic time $\hat{\tau}_{(KV)s} = \tau_{(KV)s} c_{(S)s} / H$. Eq. (20) also holds for the case of harmonic plane P-waves by substituting $c_{(S)s}$ with $c_{(P)s}$ into Eqs. (21).

In the present analysis, the amount of viscous dissipation is expressed in terms of the damping factor of the fundamental mode of the viscoelastic layer resting on a rigid bedrock:

$$\zeta = \zeta_1 = \frac{\tau_{(KV)} \omega_{s1}}{2} = \frac{\hat{\tau}_{(KV)s} \hat{\omega}_{s1}}{2} = \frac{\pi}{4} \hat{\tau}_{(KV)s}. \quad (22)$$

To validate the procedure described in Section 3, the transfer function of Eq. (20) has been numerically evaluated by finite elements. The FEM model of the viscoelastic layer on an elastic half-space is shown in Figure 6a. The horizontal size of the FEM model of the layer is twice its depth. The vertical FEM discretization of the layer comprises 32 elements to reproduce the shortest wavelengths ($\hat{\omega}_s = 4$) with sufficient accuracy.

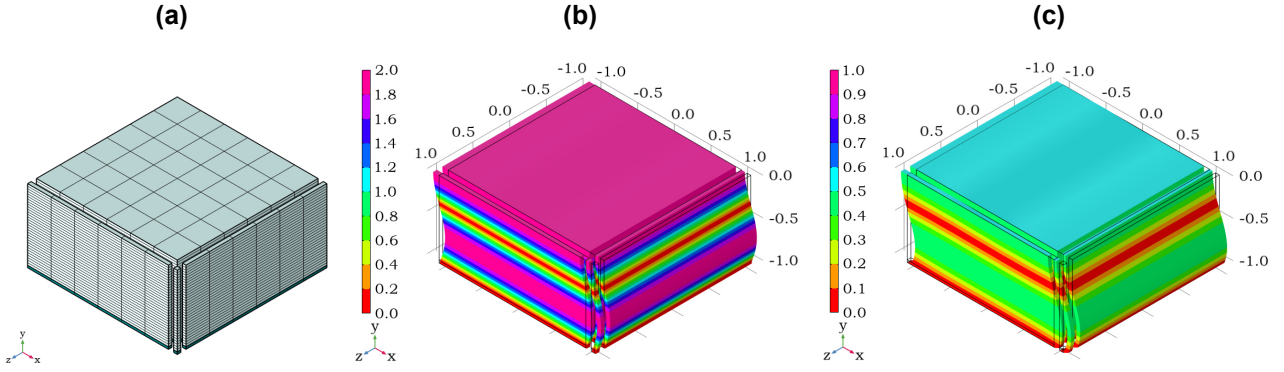


Figure 6. FEM model of a homogeneous linear viscoelastic layer lying on a linear elastic half-space (a) and displacement amplitude distribution for $\hat{\omega}_s = 1.5\pi$, $\zeta = 10^{-4}$ and $\alpha = 0.5$ (b) and $\alpha = 2.0$ (c).

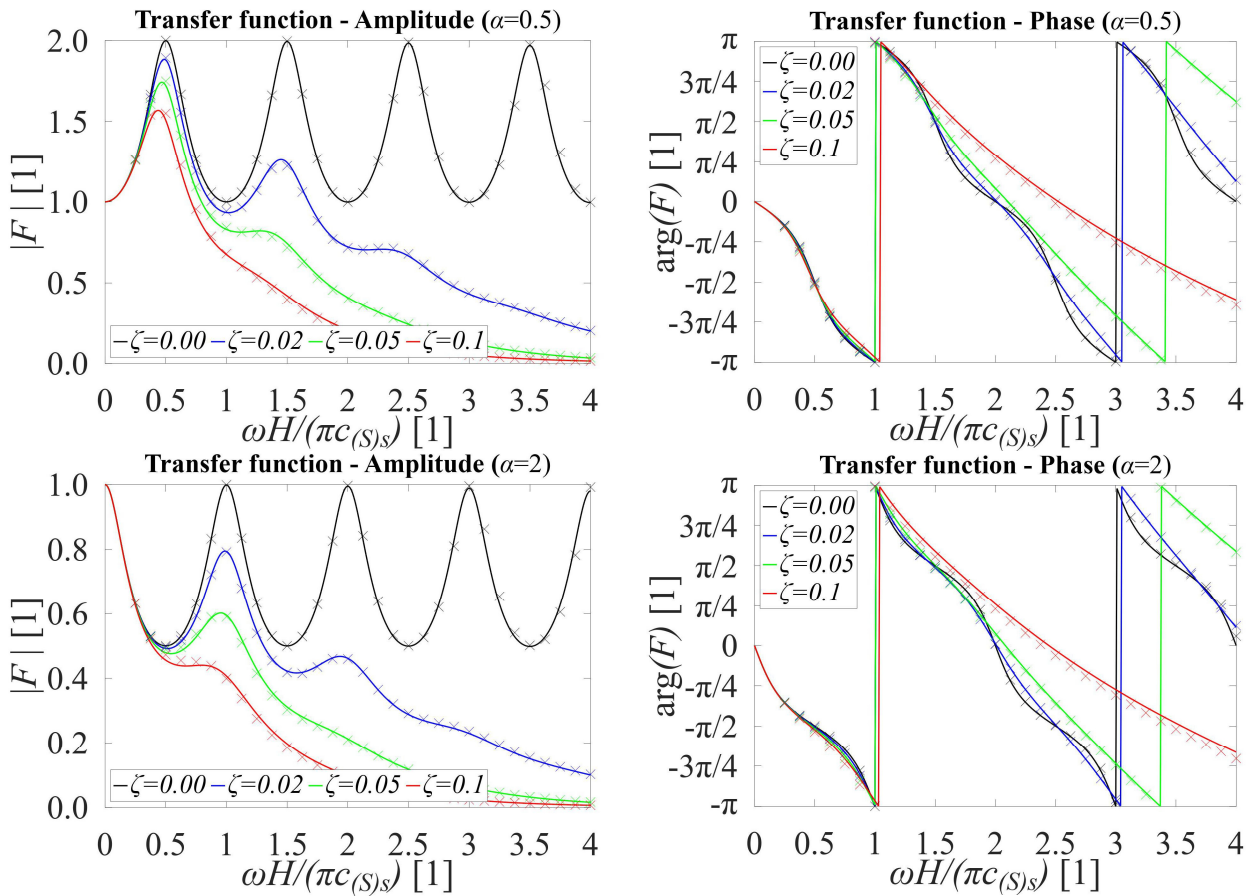


Figure 7. Amplitude and phase of transfer function of Eq. (20) and numerical results (marked by crosses) obtained by the FEM model of Figure 6a for various values of α , $\hat{\omega}_s$ and ζ .

Owing to the S-wave polarization of the seismic waves, a single FF layer only needs to be introduced for each vertical face of the interaction horizon. Moreover, since the opposite vertical faces of the artificial boundary shares the same geometry, one FF layer is sufficient for modelling the FFb for each couple of opposite faces. As a result, a single vertical column is only required to reproduce the FFb of both layers. Hence, by exploiting the symmetry of the interaction horizon and/or the directionality of the seismic input, the implementation of the DM may be much simplified as compared to the general case discussed in Section 3.

A parametric study has been carried out to validate the numerical outcomes for the following values of the characteristic parameters:

$$\alpha = \{0.5, 2\}, \quad \zeta = \{10^{-4}, 0.02, 0.05, 0.10\}, \quad 0.25\pi \leq \hat{\omega}_s \leq 4\pi; \quad (23)$$

encompassing about all practical circumstances encountered in site response analysis.

For each assigned set of parameters $\alpha, \zeta, \hat{\omega}_s$, the x -displacement amplitude and phase of the central node of the surface has been evaluated by performing a steady-state analysis in the frequency domain. Since the seismic input has unitary amplitude at the outcrop point, such x -displacement coincides with transfer function $F(\hat{\omega}_s^*, \alpha^*)$ in Eq. (20). The amplitude and phase of F versus $\hat{\omega}_s$ for various values of α and ζ are displayed in the sequence of graphs in Figure 7. The correspondence between the numerical results, drawn with crosses, and the analytical solution (continuous lines) is remarkable in the whole considered range of the characteristic parameters, thus demonstrating the excellent performances of the FFBS.

The effect of impedance ratio α in amplifying or deamplifying displacement amplitudes along the depth of the layer is depicted in Figure 6b and in Figure 6c, respectively.

4.2. Scattering of vertically propagating plane SH-waves by a semi-cylindrical canyon

Let consider a half-space having a semicylindrical indentation of radius a at its free surface. The half-space is assumed to be homogeneous, isotropic and linear elastic with shear wave velocity $c_{(S)b}$ and mass density ρ_b . The excitation of the half-space consists of vertically propagating harmonic plane SH-waves with circular frequency ω and particle motion in the z -direction with unitary amplitude at the surface.

The complex-valued transfer function of the system, i.e. the ratio between the free surface motion and the bedrock outcropping motion, as derived by Trifunac (1972), assumes this expression:

$$F(r, \theta, ka) = \begin{cases} J_0(ka) - \frac{J_1(ka)H_0^{(2)}(ka)}{H_1^{(2)}(ka)} + 2 \sum_{n=1}^{\infty} (-1)^n \left(J_{2n}(ka) - \frac{kaJ_{2n+1}(ka) - 2nJ_{2n}(ka)}{kaH_{2n+1}^{(2)}(ka) - 2nH_{2n}^{(2)}(ka)} H_{2n}^{(2)}(ka) \right) \cos(2n\theta) & |\theta| < \frac{\pi}{2} \\ J_0(kr) - \frac{J_1(ka)H_0^{(2)}(kr)}{H_1^{(2)}(ka)} + 2 \sum_{n=1}^{\infty} J_{2n}(kr) - \frac{kaJ_{2n+1}(ka) - 2nJ_{2n}(ka)}{kaH_{2n+1}^{(2)}(ka) - 2nH_{2n}^{(2)}(ka)} H_{2n}^{(2)}(kr) & |\theta| = \frac{\pi}{2} \end{cases} \quad (24)$$

where $k = \omega/c_{(S)}$ is the (angular) wave number, r e θ the coordinates of the cylindrical system centred at the canyon longitudinal axis, θ being zero along the negative y -axis and positive counter-clockwise, $J_p(\xi)$, $H_p^{(1)}(\xi)$ and $H_p^{(2)}(\xi)$ are the Bessel function of the first kind, the Hankel function of first kind and the Hankel function of second kind, respectively, with argument ξ and order p .

The above transfer function depends on the surface position (r, θ) and on the product

$$ka = \frac{\omega}{c_{(S)}} a = \pi \frac{2a}{\lambda} = \pi \xi; \quad (25)$$

expressing π times the ratio (ξ) between the canyon diameter ($2a$) and the incident SH-wavelengths (λ).

The transfer function of Eq. (24) has been numerically evaluated by applying the DM. The FEM model of the half-space with a semi-cylindrical canyon is shown in Figure 8a. The depth and the lateral extent of the mesh, assumed equal to $3a$ and $4a$, respectively, were selected by trial runs to minimize boundary reflection effects. The vertical FEM discretization of the layer comprises 36 elements to accurately approximate even the shortest wavelengths ($\xi = 2$). As for the benchmark problem discussed in the previous section, only two FF layers and a FF column are needed to appropriately enforce FFBS at all the lateral boundaries of the generalized structure.

The consistency of the numerical results has been again checked by performing a parametric analysis ($0.25\pi \leq \xi \leq 2\pi$). The computed values of the amplitude of $F(r, \theta, ka)$ are plotted along the x -axis in Figure 9. In the same figure the exact curves provided by Eq. (24) are also shown for comparison purposes. Since displacement amplitudes are symmetric with respect to the y -axis, amplification curves evaluated for $\xi \leq \pi$ are plotted only for $x \geq 0$; the remaining amplification curves ($\pi < \xi \leq 2\pi$) are plotted only for $x \leq 0$.

The numerical amplification curves satisfactorily match the target analytical ones within the whole considered range of ξ . Hence, FFBS prove to correctly work even for this more demanding benchmark problem. The spatial distribution of scattered displacement amplitudes within the half-space volume is illustrated in Figure 8b,c for two distinct values of ξ . These maps depict the increasing complexity of the scattered wave patterns as the frequency of the incident wave field increases.

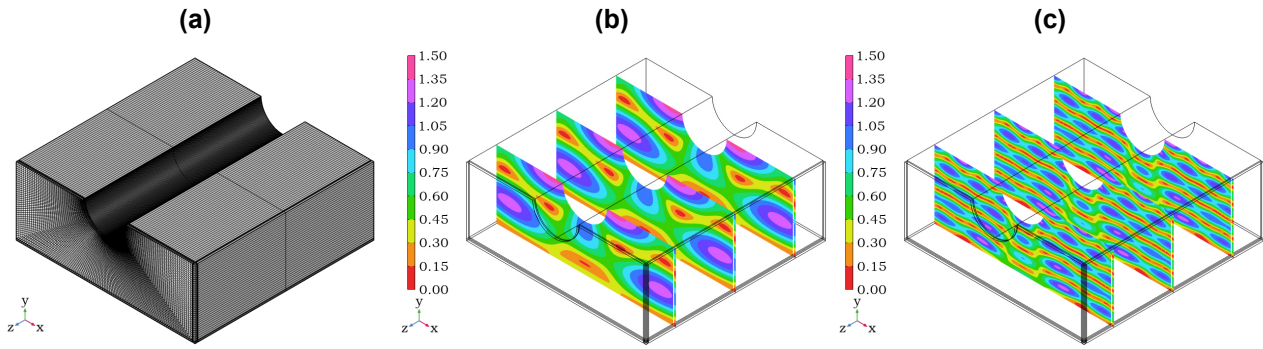


Figure 8. FEM model of a homogeneous linear elastic half-space with a semicylindrical canyon (a) and displacement amplitude distribution for $\xi = 0.25\pi$ (b) and $\xi = 0.75\pi$ (c).

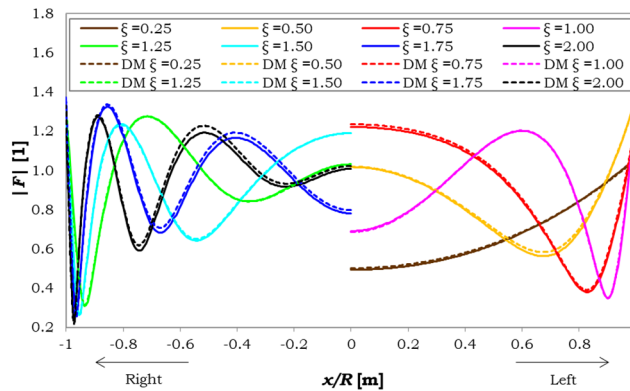


Figure 9. Transfer function amplitude of the points lying on the surface of the cylindrical canyon under vertically propagating harmonic plane SH waves for various values of $\xi = 2a/\lambda$.

5. Conclusions

In this paper, the general formulation of the DM and its implementation in COMSOL Multiphysics® commercial FEM software have been presented. The key steps needed to simulate a FFB, as required by the DM, in COMSOL Multiphysics® have been discussed in detail in Section 3. By the proposed methodology, any linear and nonlinear DSSI analysis of a dam-foundation system can be numerically solved by finite elements under the standard assumption of vertical propagation of the seismic waves from the bedrock towards the structure.

To verify the rigor of the proposed implementation of the DM, the calculated displacements have been compared against those provided by the analytical solutions of two benchmark problems. The numerical results have shown a perfect match with the analytical solution of both benchmark problems, confirming the robustness and accuracy of the present implementation of the DM. Hence, the present analysis demonstrates that rigorous DSSI analyses based on the DM can be correctly executed, even within modern commercial FEM codes, once the FFBs are correctly set up and handled. In particular, the present methodology constitutes a viable and effective tool to be used for the seismic assessment of dams, as testified by the considered examples and derived results.

Acknowledgements

The present Research & Development project on DSSI was partially supported by Enel Green Power S.r.l..

6. References

Aydinoğlu M.N. (1993). Consistent formulation of direct and substructure methods in nonlinear soil-structure interaction, *Soil Dynamics & Earthquake Engineering*, 12(7): 403-410.

Alves S.W., Hall J.F. (2006). Generation of spatially non-uniform ground motion for nonlinear analysis of a concrete arch dam, *Earthquake Engineering & Structural Dynamics*, 35(11): 1339-1357.

Chopra A.K., Wang J.-T. (2010). Earthquake response of arch dams to spatially varying ground motion, *Earthquake Engineering & Structural Dynamics*, 39: 887-906.

- Chopra A.K. (2012). Earthquake Analysis of Arch Dams: Factors to Be Considered, *ASCE Journal of Structural Engineering*, 138: 205-214.
- Chopra A.K. (2020). *Earthquake Engineering for Concrete Dams - Analysis, Design, and Evaluation*, Hoboken, NJ (USA): John Wiley & Sons Ltd.
- COMSOL Multiphysics® (2023). Version 6.1, COMSOL AB, Stockholm, Sweden.
- Froio D., Eusebio M., Bariletti A., Previtali R., Rizzi E. (2019). Direct method for dynamic soil-structure interaction based on seismic inertia forces, *Proceedings of the XV ICOLD International Benchmark Workshop on Numerical Analysis of Dams*, Milan, Italy.
- Hall J.F. (1988). The dynamic and earthquake behaviour of concrete dams: review of experimental behaviour and observational evidence, *Soil Dynamics & Earthquake Engineering*, 7(2): 58-121.
- Jin A.-Y., Pan J.-W., Wang J.-T., Zhang C. (2019). Effect of foundation models on seismic response of arch dams, *Engineering Structures*, 188: 578-590.
- Koufoudi E., Chaljub E., Dufour F., Bard P.Y., Humbert N., Robbe E. (2018). Spatial variability of earthquake ground motions at the dam-foundation rock interface of Saint Guérin: experimental and numerical investigations, *Bulletin of Earthquake Engineering*, 16: 1751-1777.
- Kramer S.L. (1996), *Geotechnical Earthquake Engineering*, Upper Saddle River, NJ (USA): Prentice Hall.
- Løkke A., Chopra A.K. (2017). Direct finite element method for nonlinear analysis of semi-unbounded dam-water-foundation rock systems, *Earthquake Engineering & Structural Dynamics*, 46(8): 1267-1285.
- Løkke A., Chopra A.K. (2018). Direct finite element method for nonlinear earthquake analysis of 3-dimensional semi-unbounded dam-water-foundation rock systems, *Earthquake Engineering & Structural Dynamics*, 47(5): 1309-1328.
- Løkke A., Chopra A.K. (2019). Direct finite element method for nonlinear earthquake analysis of concrete dams: simplification, modelling, and practical applications, *Earthquake Engineering & Structural Dynamics*, 48(7): 812-842.
- Lysmer J., Kuhlemeyer R.L. (1969), Finite dynamic model for infinite media, *Journal of Engineering Mechanics Division (ASCE)*, 95(EM4): 859-877.
- Maeso O., Aznárez J.J., Dominguez J. (2002). Effects of space distribution of excitation on seismic response of arch dams, *ASCE Journal of Engineering Mechanics*, 128(7): 759-768.
- MatLab (2022) Version R2022b. Natick, Massachusetts.
- Sánchez-Sesma F.J. (1987). Site effects on strong ground motion, *Soil Dynamics & Earthquake Engineering*, 6(2): 124-132.
- Sotoudeh P., Ghaemian M., Mohammadnezhad H. (2019). Seismic analysis of reservoir-gravity dam massed layered foundation system due to vertically propagating earthquake, *Soil Dynamics & Earthquake Engineering*, 116: 174-184.
- Szczesiak T., Weber B., Bachmann H. (1999). Nonuniform earthquake input for arch dam foundation interaction, *Soil Dynamics and Earthquake Engineering*, 18(7): 487-493.
- Trifunac M.D. (1972). Scattering of plane SH waves by a semi-cylindrical canyon, *Earthquake Engineering & Structural Dynamics*, 1(3): 267-281.
- Varmazyari M., Sabbagh-Yazdi S.-R. (2021). Modification of direct-FE method for nonlinear seismic analysis of arch dam-reservoir-foundation system considering spatially varying ground motion, *Soil Dynamics & Earthquake Engineering*, 140: 106477.
- Wang J.-T., Chopra A.K. (2010). Linear analysis of concrete arch dams including dam-water-foundation rock interaction considering spatially varying ground motions, *Earthquake Engineering & Structural Dynamics*, 39(7): 731-750.
- Wolf J.P. (1985). *Dynamic soil-structure-interaction*, Englewood Cliffs, NJ (USA): Prentice Hall.
- Wolf J.P. (1988), *Soil-structure-interaction analysis in time domain*, Englewood Cliffs, NJ (USA): Prentice Hall.
- Zienkiewicz O.C., Bicanic N., Shen F.Q. (1989). Earthquake input definition and the transmitting boundary conditions, In: *Advances in Computational Nonlinear Mechanics*, Ed. Doltsinis I. St., 109-138, Vienna, Austria: Springer-Verlag Wien.